



RESEARCH LETTER

10.1002/2016GL072346

Key Points:

- Three-dimensional attenuation images and rock properties of the crustal volume embedding the fault system associated with the destructive M_s 6.9, 1980 Irpinia earthquake
- Evidence for a fractured and fluid-saturated medium, with the presence of brine- CO_2 and CH_4 - CO_2
- Pore pressure increase is the dominant mechanisms triggering and controlling the microseismicity

Supporting Information:

- Supporting Information S1

Correspondence to:

A. Zollo,
aldo.zollo@unina.it

Citation:

Amaroso, O., G. Russo, G. De Landro, A. Zollo, S. Garambois, S. Mazzoli, M. Parente, and J. Virieux (2017), From velocity and attenuation tomography to rock physical modeling: Inferences on fluid-driven earthquake processes at the Irpinia fault system in southern Italy, *Geophys. Res. Lett.*, *44*, 6752–6760, doi:10.1002/2016GL072346.

Received 2 MAR 2016

Accepted 21 APR 2017

Accepted article online 24 APR 2017

Published online 15 JUL 2017

From velocity and attenuation tomography to rock physical modeling: Inferences on fluid-driven earthquake processes at the Irpinia fault system in southern Italy

O. Amoroso¹, G. Russo¹ , G. De Landro¹ , A. Zollo¹ , S. Garambois², S. Mazzoli³ , M. Parente³ , and J. Virieux² 

¹Department of Physics 'Ettore Pancini', University of Naples 'Federico II', Naples, Italy, ²ISTerre, Université Grenoble Alpes, CNRS, Grenoble, France, ³Department of Earth Sciences, Environment and Georesources (DiSTAR), University of Naples 'Federico II', Naples, Italy

Abstract We retrieve 3-D attenuation images of the crustal volume embedding the fault system associated with the destructive M_s 6.9, 1980 Irpinia earthquake by tomographic inversion of t^* measurements. A high Q_p anomaly is found to be correlated with the 1980 fault geometry, while the Q_s model shows regional-scale variations related to the NE edge of the uplifted pre-Tertiary limestone. An upscaling strategy is used to infer rock properties such as porosity, consolidation, type of fluid mixing, and relative saturation percentage at 8–10 km fault depth. We constrain the porosity and consolidation in the ranges 4–5% and 5–9, respectively, with the possible fluid mixes being both brine- CO_2 and CH_4 - CO_2 . The consolidation parameter range indicates high pore pressures at the same depths. These results support the evidence for a fracture system, highly saturated in gases and a seismicity triggering mechanism at the fault zone, which is strongly controlled by fluid-induced pore pressure changes.

1. Introduction

The imaging of crustal seismic velocity provides significant constraints on the physical properties of host rocks and on the potential presence of fluids, in particular in the volume embedding earthquake causative fault systems. Indeed, the contribution of pore fluid pressure changes to earthquake triggering at different rupture scales is recognized worldwide [Hardebeck and Hauksson, 1999; Husen and Kissling, 2001; Vidale and Shearer, 2006] and has been already invoked for several Italian Apennine cases [e.g., Antonioli et al., 2005; Chiarabba et al., 2011; Malagnini et al., 2012; Improta et al., 2014]. Detection, mapping, and tracking of fluid migration can notably be achieved using 4-D seismic tomography and is used especially for purposes such as oil exploration and reservoir monitoring [Lumley, 2001], understanding tectonic environments [Chiarabba et al., 2009], and volcano monitoring for short- to middle-term eruption forecasting [Patanè et al., 2006]. Fluid movements can be tracked by analyzing V_p/V_s ratio space-time changes [e.g., Lucente et al., 2010; Hamada, 2004]. However, these observables are not able to single out the type of fluid mixing and the relative percentage of saturation [Dupuy et al., 2016], which are necessary to define a reliable picture of the host rock physical properties. Attenuation tomography may provide useful and complementary insights into the physical properties of fluids, which permeate host rocks [Hauksson and Shearer, 2006].

Our study is focused on the southern Apennine area in Italy, which experienced moderate to large earthquakes in the past centuries [Rovida et al., 2016]. The largest of these, the M_s 6.9, 1980 Irpinia earthquake, occurred on an approximately 60 km long NE-SW striking normal fault segment with three main rupture episodes [Bernard and Zollo, 1989]. The crustal extensional stress regime controls earthquake generation processes in the mountain chain. Background seismicity is characterized by microearthquakes ($M_L < 3.5$) approximately confined within the same volume wherein the faults, which caused the 1980 earthquake and its aftershocks, were located [Matrullo et al., 2013; De Landro et al., 2015]. It delineates a system of northwest-southeast striking normal faults along the Apennine chain and an approximately east-west oriented strike-slip fault transversely cutting the belt (Figure 1a) [De Matteis et al., 2012]. Surface faults exposed in this area are decoupled from the seismically active deep-seated structures, which in turn reactivate inherited basement faults [Ascione et al., 2013]. Effective decoupling between deep and

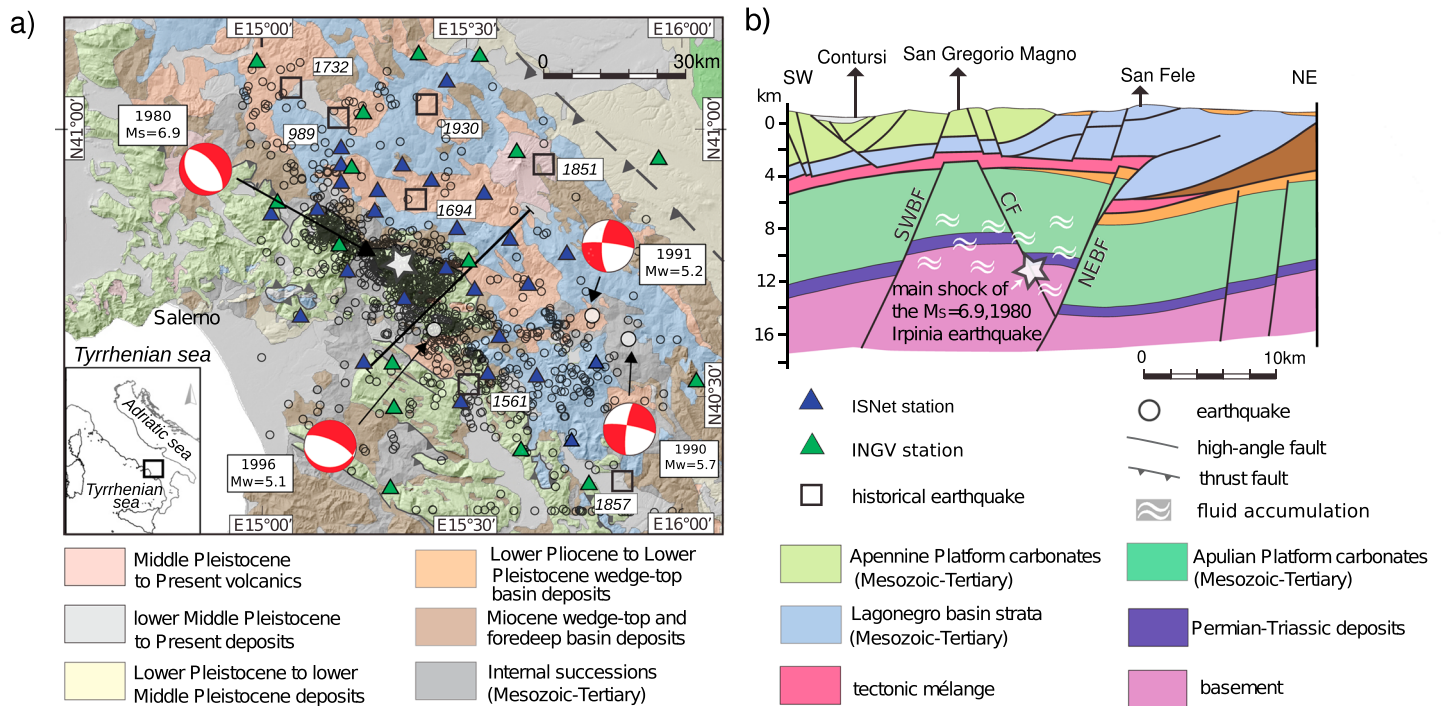


Figure 1. Tectonic setting of the southern Apennines [after Ascione *et al.*, 2013]. (a) Geological sketch map. Black squares indicate the location of the main historical and instrumental earthquakes. Black circles indicate the events used in this study. (b) Geological cross section along the profile reported in the map in Figure 1a; SWBF: SW boundary fault; CF: central fault; NEBF: NE boundary fault.

shallow structural levels is related to the strong rheological contrast produced by the fluid-saturated, clay-rich melange zone interposed between the foreland Apulia platform carbonates and the allochthonous units (Figure 1).

According to Amoroso *et al.* [2014], the high-resolution 3-D *P* and *S* wave velocity models of the Irpinia fault zone highlight a significant fluid accumulation within a 15 km wide volume of highly fractured rock located between SW (SWBF) and NE (SWBF) boundary faults as indicated in Figure 1b. The background microseismicity was therefore attributed to pore pressure changes in fluid-filled cracks surrounding major faults, which can trigger the episodic nucleation of moderate to large earthquakes. Analyses of microearthquake sequences revealed that they are primarily concentrated in densely fractured and limited regions that could be the source of repeated earthquakes due to the internal mechanical readjustments from local stress release and/or fluid migration along the fault zone [Stabile *et al.*, 2012].

Here we propose to use the estimates of tomographic velocity and attenuation values to retrieve information about porosity, the type of permeating fluids, saturation percentage, and consolidation parameter through established rock physical laws, thus providing a comprehensive seismic interpretation of the Irpinia fault zone. We performed an attenuation tomographic inversion, which provides 3-D images of the anelastic attenuation properties in terms of body wave quality factors (Q_p and Q_s). These quantitative images complement the already existing velocity images inferred from local earthquake tomography [Amoroso *et al.*, 2014]. The possible range of porosity and relative saturation of host rocks (microparameters) is determined from the retrieved ranges of velocity and attenuation (macroparameters) through a systematic exploration based on an upscaling procedure.

2. Attenuation Tomography: Data, Method, and Inversion Strategy

Seismic waves propagating across the Earth undergo energy dissipation processes, which cause the amplitude to decrease as a function of the traveled distance and the wave frequency. The parameter describing the anelastic attenuation is the quality factor Q , whose reciprocal is proportional to the relative fraction of

energy dissipated for frictional mechanisms in a wave cycle [Lay and Wallace, 1995]. Q is in turn linked to the observed parameter t^* via the formula

$$t^* = \int_i^j \frac{dl}{vQ} \quad (1)$$

where v is the velocity of the medium and dl is the distance along the raypath from hypocenter i to station j [Rietbrock, 2001].

We used the t^* measurements obtained by Zollo *et al.* [2014], who applied a spectral fitting technique to microearthquake P and S waveforms, and found that in the analyzed frequency band an attenuation model with constant Q is preferred to frequency-dependent Q models (more details in the supporting information) [Boatwright, 1980; Morozov, 2008].

We selected the best located events in the 3-D velocity model of Amoroso *et al.* [2014] among those that occurred from August 2005 to April 2011 and were recorded by the stations operated by the University of Naples ISNet (Irpina Seismic Network, AMRA) and INGV (Istituto Nazionale di Geofisica e Vulcanologia) (Figure 1). We thereby analyzed a data set of 4801 t_p^* and 1833 t_s^* relative to 670 earthquakes with local magnitude $0.1 \leq M_L \leq 3.2$.

In order to perform the 3-D attenuation tomography, we used a modified version of the code originally used by Amoroso *et al.* [2014] to perform the delay time inversion. We inverted the t^* data for Q following a *multi-scale* strategy [Chiao and Kuo, 2001; Zollo *et al.*, 2002] whereby several optimization runs are performed by progressively increasing the density of grid points describing the attenuation model (more details in the supporting information) [Latorre *et al.*, 2004]. We used three different grids spacing equal to $12 \times 12 \times 4 \text{ km}^3$ (parametrization A), $6 \times 6 \times 2 \text{ km}^3$ (parametrization B), and $3 \times 3 \times 1 \text{ km}^3$ (parametrization C). Ray tracing was performed using the Amoroso *et al.* [2014] models. The t_p^* and t_s^* were inverted independently. The starting model was obtained by parameterizing the medium with a very coarse grid in the horizontal directions with respect to the vertical and using a homogeneous model, whose values corresponded to the median ones estimated by Zollo *et al.* [2014], e.g., $Q_p = 167$ and $Q_s = 226$. The starting model was obtained by averaging the values at the nodes located at the same depth. We selected the optimal damping parameter by using the empirical approach of Eberhart-Phillips [1986]. The smoothing of the solution was achieved by constraining the Laplacian of the attenuation field to be 0 [Benz *et al.*, 1996].

To identify the high-resolution and low-smearing model regions, we computed the *derivative weight sum* (DWS), which measures the ray density in the neighborhood of every node [Hauksson and Shearer, 2006]. The threshold value of DWS delimiting the well-resolved area was calibrated by comparing the diagonal elements of the resolution matrix and the spread function [Michellini and McEvilly, 1991]. This comparison was made only for the parametrizations A and B, since the resolution matrix for parameterization C could not be computed due to the large model size.

3. Modeling of Rock Physical Properties

We considered another inverse problem where the retrieved seismic velocities and attenuations (macroparameters) were our input data set. From these observables, we recovered the properties of the host rock volume characterized by a set of microparameters (porosity, consolidation parameter, permeating fluid type, and percentage of fluid saturation), which describe the hydrological properties of the solid and biphasic fluid components. We did this by an exhaustive sampling of microparameters for a prediction of macroparameters resulting from an upscaling strategy. This procedure relies on the rock model developed by Pride [2005], based on the Biot's [1962] theory of poroelasticity [Dupuy *et al.*, 2016] and Gassmann's relation [Gassmann, 1951] that provide the bulk modulus of the drained medium during a fluid substitution. More details on methodology can be found in the supporting information and literature studies [Wyllie *et al.*, 1956; Dvorkin *et al.*, 1995; Brocher, 2005; Burrige and Vargas, 1979; Mavko *et al.*, 2009; Brie *et al.*, 1995]. In particular, the consolidation parameter (C_c) describes the degree of consolidation of solid matrix grains, larger values representing less consolidated rocks [Pride, 2005]. We focused our rock physics modeling on the volume embedding the Irpinia fault system between 8 and 10 km depth, where the quality factor Q_p ranges between 350 and 850 (see Figures 2 and 3) and where most of the present seismicity occurs. By direct comparison between

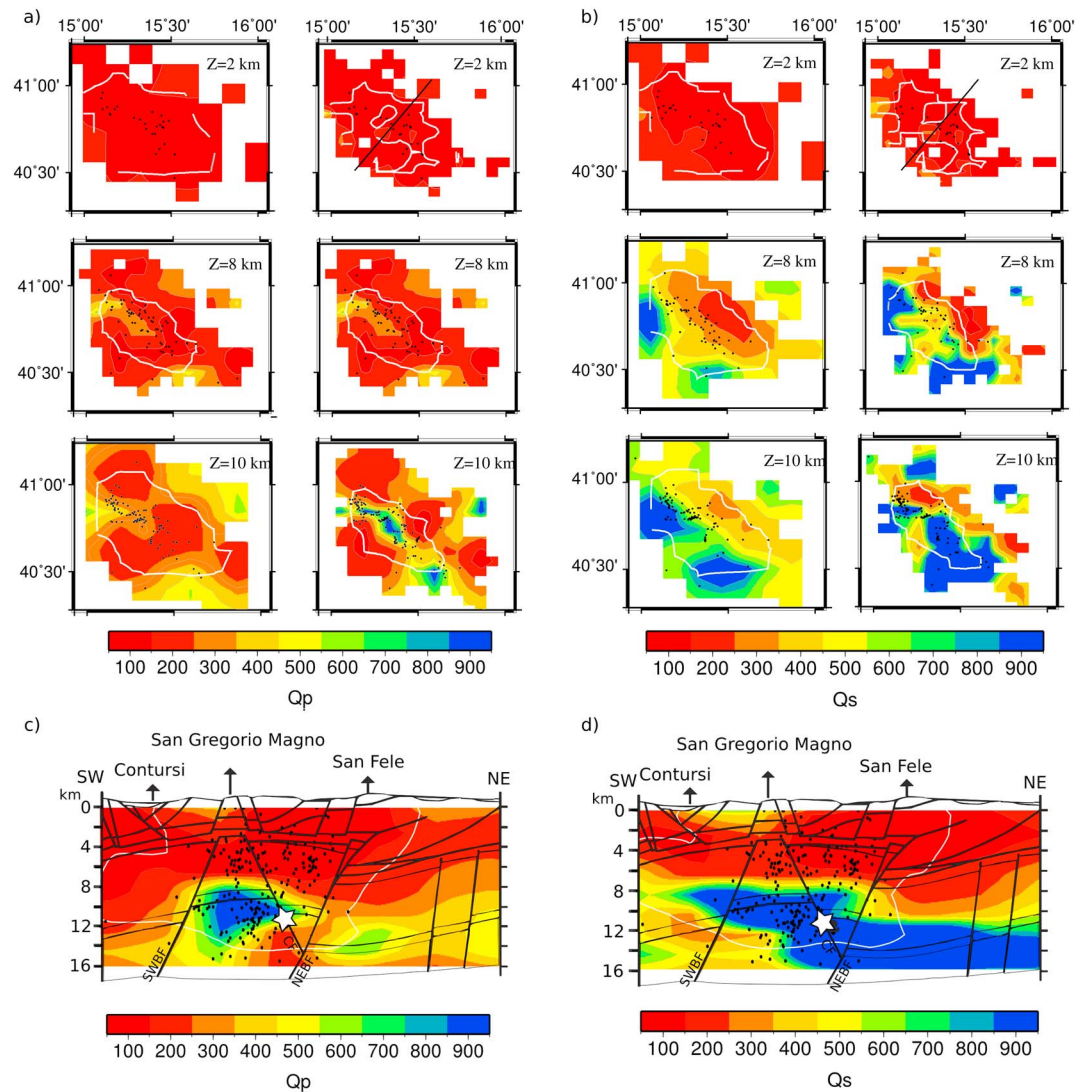


Figure 2. Three-dimensional attenuation models. (a) Q_p and (b) Q_s horizontal slices for parametrization A (left column) and B (right column). White curves delimit the well-resolved model regions according to the DWS. Black dots represent the earthquakes located in a range of 1 km around each layer depth. (c) Q_p and (d) Q_s models, for parameterization B, and microearthquake locations projected onto the cross section located in Figure 1a (refer to Figure 1b for the tectonic contacts). White curves delimit the well-resolved regions.

the upscaled values describing theoretical macroparameters and those inferred from the velocity and attenuation tomography, we infer bound values of microparameters for the area enclosed within the SWBF and NEBF (Figures 1 and 2). For this, we needed to restrict the number of poroelastic parameters by assuming the lithology of the host rock, the range of variability for porosity and C_s , and the type of fluids to include in the modeling.

Cross-Appennine seismic profiles [Mostardini and Merlini, 2004] indicate that the investigated depth range host—for the most part—the lower portion of the Apulian platform and, for a smaller thickness, the underlying clastic sediments and the basement. Three oil wells drilled in the considered area (Contursi, San Gregorio Magno, and San Fele; see Figure 1b) did not reach the lower part of the Apulia carbonate platform. However, two deep boreholes, drilled for oil exploration in the Apulia region to the east, i.e., the Gargano 1 and Puglia 1 wells (available from the ViDEPI Project at <http://unmig.sviluppoeconomico.gov.it/videpi/pozzi/pozzi.asp>), indicate that the lower part of the Apulia carbonate platform is mainly formed of dolostones. Therefore, we used dolomite as the dominant mineral component for our rock physical modeling.

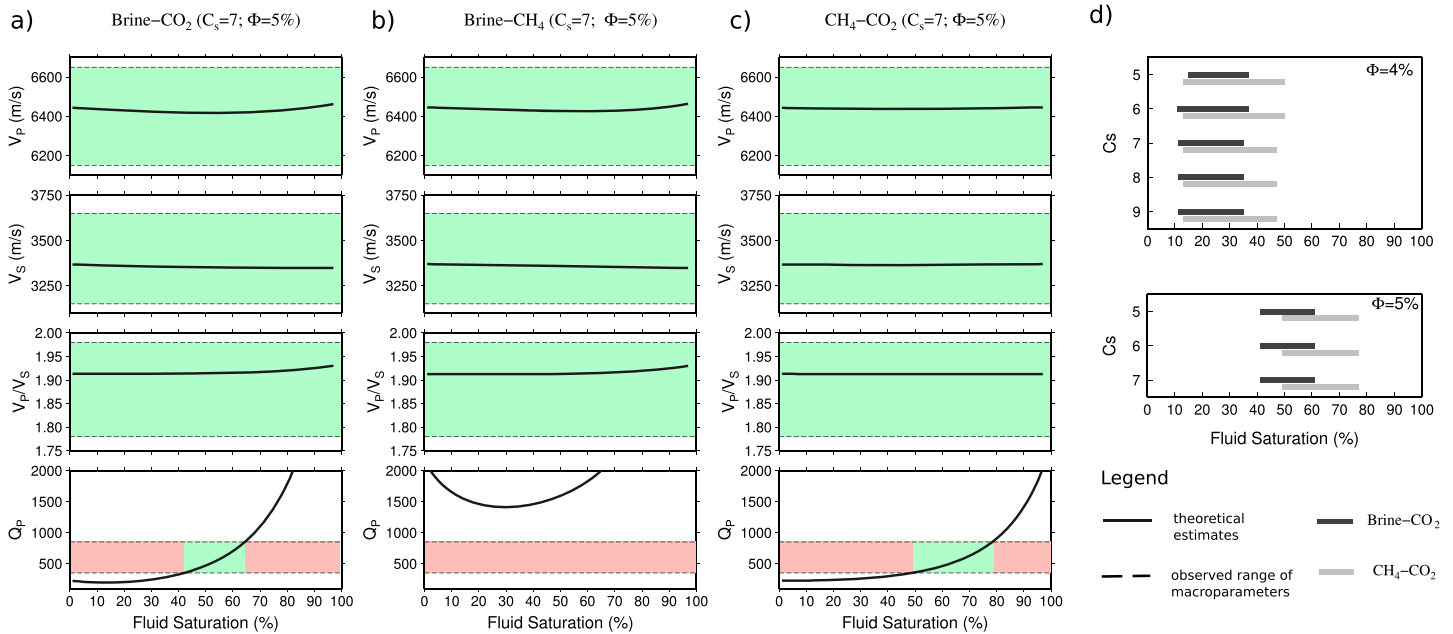


Figure 3. Upscaling results. (a–c) Macroparameters derived from upscaling as a function of relative fluid saturation (percentage of the first fluid phase with respect to the second) for the three tested fluid couples and different combinations of Φ (porosity) and C_s . The black dashed lines delimit the range of the retrieved values from the tomographic images. The ranges are green when the upscaled curves fall inside the retrieved range, while they are red otherwise. (d) Saturation ranges for which the upscaled curves fall inside the retrieved range by varying C_s and considering $\Phi = 4\%$ (top) and $\Phi = 5\%$ (bottom).

In the Puglia 1 well, porosity values ranging between 0.87% and 2.53% have been measured in the dolostones of the Burano formation at 5 km depth. Another core taken at 6 km depth in alternating dolostones and anhydrites provided a porosity range of 0.70–1.37%. Larger values of porosity have been reported for carbonate reservoirs (limestones and dolostones) in the same depth interval. The modal value of average porosity at a depth of 5.25–5.75 km in the huge data set of *Ehrenberg and Nadeau* [2005] is 6.2%. For greater depths, the empirical relation of *Schmoker and Halley* [1982] can be used to predict a porosity of 3.5% for dolostone at a depth of 8 km. Most of the porosity values used for the previously cited studies are derived from core measurements or well log analyses. The total porosity at the scale considered for our modeling can be significantly higher due to the likely presence of dense networks of fractures [*Amoroso et al.*, 2014]. For this reason, the explored range of porosity was extended up to 5% in the inversion process.

According to *Pride* [2005], C_s values range from 2 to 20 in sandstones. *De Ceia et al.* [2015] estimated C_s for a set of microporous carbonate rocks and showed that its values fall, for the most part, within the range indicated for sandstone. *Lee* [2005] concluded that, in practice, C_s could be viewed as a free parameter to fit the data if both porosity and P and S wave velocities are known. Therefore, in our upscaling procedure, we explored the entire [2, 20] range for C_s , expecting that the comparison with the retrieved macroparameters could better constrain it.

We hypothesize that the fluids permeating the rocks at the investigated depths are brine, CO₂, and CH₄ based on recent measurements of gas emission at surface [*Inversi et al.*, 2013; *Chiodini et al.*, 2004; *Ciotoli et al.*, 2014]. We excluded the steam phase since brine can only exist in the liquid phase at temperature and pressure conditions within the considered depth range. Similarly, we did not consider oil as a plausible permeating fluid since only very minor impregnations have been found in the San Gregorio Magno well (as it results from the ViDEPI Project). The modeling assumes an incident wave with a 20 Hz predominant frequency, which is consistent with the range of observed source characteristic frequencies (5–30 Hz) of microearthquakes [*Zollo et al.*, 2014].

Gassmann's relation requires that the shear modulus of the saturated rock be the same as that of the dry rock. However, *Adam et al.* [2006] showed that the shear modulus, which is linked to Q_s , decreases in water-saturated rock samples, so the assumption that it is independent of the fluid substitution may not be valid

Table 1. Summary of the Results Obtained From the Comparison Between the Upscaled Macroparameters Curves and the Retrieved Macroparameters Ranges^a

C_s	4				5				6				7				8				9				10					
	2	3	4	5	2	3	4	5	2	3	4	5	2	3	4	5	2	3	4	5	2	3	4	5	2	3	4	5		
V_p	X	X	X	X	X	X	✓	✓	X	X	✓	✓	X	✓	✓	✓	X	✓	✓	✓	X	X	✓	✓	✓	X	X	✓	X	X
V_s	X	✓	✓	X	X	✓	✓	✓	X	✓	✓	✓	X	✓	✓	✓	X	✓	✓	✓	X	X	✓	✓	✓	X	X	✓	X	X
V_p/V_s	✓	✓	✓	✓	✓	✓	✓	✓	✓	✓	✓	✓	✓	✓	✓	✓	✓	✓	✓	✓	✓	✓	✓	✓	✓	✓	✓	✓	✓	✓
Q_p	-	-	-	-	-	-	✓	✓	-	-	✓	✓	-	X	✓	✓	-	X	✓	✓	-	-	X	✓	-	-	X	-	-	-

^aThe checkmark indicates that all upscaled curves fall in the retrieved range; otherwise, a cross is present. The dash indicates that the value is not reported because the velocity curve falls outside the retrieved range.

for carbonate rocks in the range of seismic frequencies. Instead, the bulk modulus, which is linked to Q_p , is well predicted by the Gassman’s relations that we adopted; therefore, we did not consider the Q_s parameter for the rock physics interpretation.

In summary, we assumed that the simulated rock has a dominant dolomite mineralogical composition, a porosity in the range [1%, 5%], and C_s in [2, 20], and we considered pores and fractures filled by a two-phase fluid (brine- CO_2 , brine- CH_4 , and CH_4 - CO_2). We then computed the values of the macroparameters (V_p , V_s , and Q_p) by varying the relative saturation percentage and compare them to the observed values.

4. Results

The retrieved attenuation models have the root mean square value of residuals showing a reduction of 34% for the Q_p inversion and 39% for the Q_s inversion relative to the initial reference models (see Figure S2 of the supporting information).

According to the resolution analysis, the extent of the best-resolved volumes depends on the chosen parameterization and generally decreases as the grid step decreases (see Figures S3–S5 in the supporting information). The well-resolved areas have been outlined using the DWS. These values show that Q_p and Q_s are well resolved from 0 to 14.5 km depth for the A and B parameterizations, while the well-resolved area is less extended for C parameterization and ranges from 2.5 to 10.5 km depth. For this reason, hereinafter only the results for the A and B will be commented, while the results for C are shown in the supporting information.

The horizontal sections through the Q_p and Q_s models show regional-scale, lateral variations in the direction perpendicular to the Apennine chain (Figures 2a and 2b). The Q_p model with parameterization A shows a slight increase of the values with depth, while with parameterization B the increase with depth is sharper, with values ranging from 350 to 850 in the central part of the model, confined between the boundary faults at depths between 8 and 12 km (Figure 2c). This high Q_p anomaly is spatially correlated with the fault structure associated with the 1980 Irpinia earthquake. The Q_s model also shows, with both parameterizations, strong lateral variations along a SW-NE section with a major transition occurring in correspondence with the 1980 earthquake rupture and the northeastern edge of the uplifted pre-Tertiary limestone. In its cross-section representation with parameterization B (Figure 2d), the Q_s model clearly delineates the transition between the carbonate-dominated sedimentary cover and the basement at about 7 km depth with an increase of values from 400 to 950.

We then matched the tomographic macroparameters with those calculated using the upscaling procedure previously described. We defined a likely set of microparameters for which the resulting upscaled macroparameters fall within the range of the retrieved values. We also determined the range of retrieved macroparameters through the analysis of the statistical distributions of velocity and attenuation in the considered depth volume (see supporting information). We selected the macroparameter values (V_p , V_s , V_p/V_s , and Q_p) falling within the volume bounded by SWBF and NEBF, as indicated in Figure 2 and extending north for about 10 km. The limiting values for macroparameters are those for which the cumulative frequency ranged between 15% and 85%. From Table 1, we infer a porosity range of 4% to 5% and a C_s between 5 and 9 for the host rock. Concerning the fluid combinations, both brine- CO_2 and CH_4 - CO_2 are possible at 8–10 km

depth with a different combination of porosity and C_s (Figures 3a and 3c), while the combination brine-CH₄ is not (Figure 3b). This result indicates that the most likely fluid mixing is CO₂ in combination with brine or CH₄.

Figure 3d shows relative fluid saturation for different values of C_s and porosity. The relative fluid saturation percentage is independent of C_s but depends on porosity. This does not allow us to discriminate whether one of the two fluids has a dominant saturation percentage in the explored rock volume. However, considering the lower porosity of 4% (Figure 3d, bottom), the relative saturation indicates a prevalence of CO₂.

Finally, the upscaled V_p/V_s ratio falls always within the range of the retrieved value, slightly increasing with saturation, for all the porosity and C_s values. This ratio appears weakly sensitive to the type of fluid combination (Figures 3a–3d).

5. Discussion and Conclusions

The strong lateral SW-NE variation of Q_s coincides with the NW-SE trending lateral velocity discontinuity previously revealed by *Amato et al.* [1992] and recently confirmed by *Amoroso et al.* [2014] and *Improta et al.* [2014], affecting the shallow upper crustal volume across the Irpinia earthquake fault zone. This discontinuity can be associated with the contrast between the thick cover of low-velocity, high-attenuation Miocene basin sediments to the NE and the high-velocity, low-attenuation carbonate outcrops of the Apennine platform to the SW [*Ascione et al.*, 2013]. This result suggests that jointly mapping Q_s seismic velocities in 3-D allows to constrain the geometrical features of large-scale geological structures and lithological transitions. On the other hand, due to its specific high-frequency content, Q_p detects the smaller wavelength spatial variation, e.g., in our study, the fine location and geometry of the 1980 earthquake fault.

The V_p and V_s values are needed to constrain the range of average, rock volume porosity, but their curves for different fluid combinations, keeping porosity and C_s fixed, have the same trend and all fall within the observed range of macroparameters (Figures 3a–3c). This means that V_p , V_s , and their ratio alone cannot discriminate between the type and different combinations of fluid phases within the uncertainties of the observed macroparameters and modeling. On the other hand, Q_p provides a stronger constraint on rock physical microparameters, allowing to reject the fluid mixings that exhibit upscaled theoretical values well outside the uncertainty bounds.

The determined porosity range (4 to 5%) at a depth of 8–10 km is larger than that measured from borehole rock samples (1–2%). This can be justified by assuming a significant contribution of a densely fractured system to the porosity at the mesoscale as proposed by *De Matteis et al.* [2012] and *Amoroso et al.* [2014].

De Ceia et al. [2015] retrieved a relation between the C_s and effective pressure through indirect measurements on carbonate rock samples. They found that C_s decreased as the effective pressure increased. By using this relation and considering a standard gradient for the overburden pressure, we found that at 8–10 km depth our C_s values correspond to a pore pressure of up to about 150 MPa. These inferred pore pressure values are significantly high and support the hypothesis of seismic fracture generation driven by pore pressure changes in the fault zone.

As for the possible fluid mixes, both brine-CO₂ and CH₄-CO₂ are compatible with observed macroparameters, thus supporting the presence of gasses CO₂ and/or CH₄ at the explored depth range. We suggest that these gasses whose emissions are both observed at Earth surface can be trapped just below and/or in the lower part of the Apulian platform, within dolostones sealed by anhydrite levels [*Trippetta et al.*, 2013], fed by fluid-rich mantle melts intruded into the crust [e.g., *Improta et al.*, 2014] and associated magma-carbonate interaction (e.g., decarbonation).

The presence of liquid and gas fluid phases in a fault volume and the inferred high pore pressure values have important consequences on seismicity generation. In fact, the presence of fluids inside the fault gauge may enhance seismicity due to lubrication mechanisms and by an increase of pore pressure in the medium embedding the faults. In the Irpinia fault zone, the modeling of microearthquake spectra has provided a rather low average seismic radiation efficiency [*Zollo et al.*, 2014], thus implying that the rupture lubrication mechanisms are not favored. Therefore, we suggest that the dominant mechanism triggering the microseismicity at the Irpinia fault zone is the pore pressure increment, induced by fluid diffusion in the host rock medium [*Dvorkin et al.*, 2000; *Shapiro et al.*, 2003]. When rocks are close to a critical

state of failure, a perturbation of the pore pressure, modifying the effective normal stress, can lead to the occurrence of a seismic fracture [Nur and Booker, 1972]. In particular, at the considered depths, gasses more than liquids may significantly increase the pore pressure up to a level for which it equals the lithostatic pressure [Hantschel and Kauerauf, 2009]. The results of the upscaling procedure, especially in terms of C_s , allow us to interpret the investigated volume at 8–10 km depth as highly fractured and liquid-gas saturated, where the high pore pressure is directly responsible for the seismicity triggering mechanism and where, in fact, most of seismicity occurs.

Acknowledgments

Zollo is responsible for the t^* data set available from his previous work quoted in references. Data are available for academic purposes upon request. This work was supported by a Post-Doctoral Fellowship at the University of Naples, Federico II, and was partially funded by Project EPOS (GA 676564-H2020-INFRADEV-2014-2015) and EU Project SHEER (GA 640896).

References

- Adam, L., M. Batzle, and I. Brevik (2006), Gassmann's fluid substitution and shear modulus variability in carbonates at laboratory seismic and ultrasonic frequencies, *Geophysics*, *71*(6), F173–F183, doi:10.1190/1.2358494.
- Amato, A., C. Chiarabba, L. Malagnini, and G. Selvaggi (1992), Three-dimensional P -velocity structure in the region of the $M_s = 6.9$ Irpinia, Italy, normal faulting earthquake, *Phys. Earth Planet. In.*, *75*, 111–119.
- Amoroso, O., A. Ascione, S. Mazzoli, J. Virieux, and A. Zollo (2014), Seismic imaging of a fluid storage in the actively extending Apennine mountain belt, southern Italy, *Geophys. Res. Lett.*, *41*, 3802–3809, doi:10.1002/2014GL060070.
- Antonoli, A., D. Piccinini, L. Chiaraluce, and M. Cocco (2005), Fluid flow and seismicity pattern: Evidence from 1997 Umbria-Marche (central Italy) seismic sequence, *Geophys. Res. Lett.*, *32*, L10311, doi:10.1029/2004GL022256.
- Ascione, A., S. Mazzoli, P. Petrosino, and E. Valente (2013), A decoupled kinematic model for active normal faults: Insights from the 1980, $M_s = 6.9$ Irpinia earthquake, southern Italy, *Geol. Soc. Am. Bull.*, *125*, 1239–1259, doi:10.1130/B30814.1.
- Benz, H., B. Chouet, P. Dawson, J. Lahr, R. Page, and J. Hole (1996), Three-dimensional P and S wave velocity structure of Redoubt Volcano, Alaska, *J. Geophys. Res.*, *101*, 8111–8128.
- Bernard, P., and A. Zollo (1989), The Irpinia (Italy) 1980 earthquake: Detailed analysis of a complex normal faulting, *J. Geophys. Res.*, *94*(B2), 1631–1647.
- Boatwright, J. (1980), A spectral theory for circular seismic sources: Simple estimates of source dimension, dynamic stress drop and radiated energy, *Bull. Seism. Soc. Am.*, *70*(1), 1–27.
- Burrige, R., and C. A. Vargas (1979), The fundamental solution in dynamic poroelasticity, *Geophys. J. Int.*, *58*(1), 61–90.
- Biot, M. A. (1962), Mechanics of deformation and acoustic propagation in porous media, *J. Appl. Phys.*, *33*(4), 1482–1498.
- Brie, A., F. Pampuri, A. F. Marsala, and O. Meazza (1995), Shear sonic interpretation in gas-bearing sands, in *Proceeding of the SPE Annual Technical Conference and Exhibition*, SPE30595, Dallas, Tex., 22–25 Oct.
- Brocher, T. M. (2005), Empirical relations between elastic wavespeeds and density in the Earth's crust, *Bull. Seismol. Soc. Am.*, *95*(6), 2081–2092.
- Chiao, L.-Y., and B.-Y. Kuo (2001), Multiscale seismic tomography, *Geophys. J. Int.*, *145*, 517–527.
- Chiarabba, C., P. De Gori, and E. Boschi (2009), Pore-pressure migration along a normal fault system resolved by time-repeated seismic tomography, *Geology*, *37*, 67–70, doi:10.1130/G25220A.1.
- Chiarabba, C., P. De Gori, and A. Amato (2011), Do earthquake storms repeat in the Apennines of Italy?, *Terra Nova*, *00*(0), 1–7, doi:10.1111/j.1365-3121.2011.01013.x.
- Chiodini, G., C. Cardellini, A. Amato, E. Boschi, S. Caliro, F. Frondini, and G. Ventura (2004), Carbon dioxide Earth degassing and seismogenesis in central and southern Italy, *Geophys. Res. Lett.*, *31*, L07615, doi:10.1029/2004GL019480.
- Ciotoli, G., S. Bigi, C. Tartarello, P. Sacco, S. Lombardi, A. Ascione, and S. Mazzoli (2014), Soil gas distribution in the main coseismic surface rupture zone of the 1980, $M_s = 6.9$, Irpinia earthquake (southern Italy), *J. Geophys. Res. Solid Earth*, *119*, 2440–2461, doi:10.1002/2013JB010508.
- de Ceia, M. A. R., R. M. Misságia, I. L. Neto and N. Archilha (2015), Relationship between the consolidation parameter, porosity and aspect ratio in microporous carbonate rock, *J. Appl. Geophys.*, *122*, 11–21, doi:10.1016/j.jappgeo.2015.09.012.
- De Landro, G., O. Amoroso, T. A. Stabile, E. Matrullo, A. Lomax, and A. Zollo (2015), High precision differential earthquake location in 3D models: Evidence for a rheological barrier controlling the micro-seismicity at the Irpinia fault zone in southern Apennines, *Geophys. J. Int.*, *203*, 1821–1831, doi:10.1093/gji/ggv397.
- De Matteis, R., E. Matrullo, L. Rivera, T. A. Stabile, G. Pasquale, and A. Zollo (2012), Fault delineation and regional stress direction from the analysis of background microseismicity in the southern Apennines, Italy, *Bull. Seismol. Soc. Am.*, *102*, 1899–1907, doi:10.1785/0120110225.
- Dupuy, B., A. Asnaashari, R. Brossier, S. Garambois, L. Métivier, A. Ribodetti, and J. Virieux (2016), A downscaling strategy from FWI to microscale reservoir properties from high-resolution images, *Lead. Edge*, *35*(2), 146–150, doi:10.1190/tle35020146.1.
- Dvorkin, J., G. Mavko, and A. Nur (1995), Squirt flow in fully saturated rocks, *Geophysics*, *60*(1), 97–107.
- Dvorkin, J., M. B. Helgerud, W. F. Waite, S. H. Kirby, and A. Nur (2000), Introduction to physical properties and elasticity models, in *Natural Gas Hydrate*, pp. 245–260, Springer, Netherlands.
- Eberhart-Phillips, D. (1986), Three dimensional velocity structure in northern California coast ranges from inversion of local earthquake arrival times, *Bull. Seismol. Soc. Am.*, *76*(4), 1025–1052.
- Ehrenberg, S. N., and P. H. Nadeau (2005), Sandstone vs. carbonate petroleum reservoirs: A global perspective on porosity-depth and porosity-permeability relationships, *AAPG Bull.*, *89*(4), 435–445, doi:10.1306/11230404071.
- Gassmann, F. (1951), Elasticity of porous media, *Vierteljahrsschrder Naturforschenden Gessellschaft*, *96*, 1–23.
- Hamada, G. M. (2004), Reservoir fluids identification using V_p/V_s ratio, *Oil Gas Sci. Technol.-Rev. IFP*, *59*(6), 649–654.
- Hantschel, T., and A. I. Kauerauf (2009), *Fundamentals of Basin and Petroleum Systems Modeling*, XVI, 476, Springer, Berlin, doi:10.1007/978-3-540-72318-9.
- Hardebeck, L., and E. Hauksson (1999), Role of fluids in faulting inferred from stress field signature, *Science*, *285*, 236–239.
- Hauksson, E., and P. M. Shearer (2006), Attenuation models (Q_p and Q_s) in three dimensions of the Southern California crust: Inferred fluid saturation at seismogenic depths, *J. Geophys. Res.*, *111*, B05302, doi:10.1029/2005JB003947.
- Husen, S., and E. Kissling (2001), Postseismic fluid flow after the large subduction earthquake of Antofagasta, Chile, *Geology*, *29*(9), 847–850, doi:10.1130/0091.
- Improta, L., P. De Gori, and C. Chiarabba (2014), New insights into crustal structure, Cenozoic magmatism, CO_2 degassing, and seismogenesis in the southern Apennines and Irpinia region from local earthquake tomography, *J. Geophys. Res. Solid Earth*, *119*, 8283–8311, doi:10.1002/2013JB010890.

- Inversi, B., et al. (2013), 3D geological modelling of a fractured carbonate reservoir for the study of medium enthalpy geothermal resource in the Southern Apennines (Campania Region, Italy), In Extended abstract, European Geothermal Congress.
- Latorre, D., J. Virieux, T. Monfret, V. Monteiller, T. Vanorio, J. L. Got, and H. Lyon-Caen (2004), A new seismic tomography of Aigion area (Gulf of Corinth, Greece) from the 1991 data set, *Geophys. J. Int.*, *159*, 1013–1031, doi:10.1111/j.1365-246X.2004.02412.x.
- Lay, T., and T. C. Wallace (1995), *Modern Global Seismology*, pp. 104–120, Academic Press, New York.
- Lee, M. W. (2005), Proposed moduli of dry rock and their application to predicting elastic velocities of sandstones, *Sci. Invest. Rep.* 2005-5119.
- Lucente, F. P., P. De Gori, L. Margheriti, D. Piccinini, M. Di Bona, C. Chiarabba, and N. P. Agostinetti (2010), Temporal variation of seismic velocity and anisotropy before the 2009 M_w 6.3 L'Aquila earthquake, Italy, *Geology*, *38*, 1015–1018, doi:10.1130/G31463.1.
- Lumley, D. E. (2001), Time-lapse seismic reservoir monitoring, *Geophysics*, *66*, 50–53, doi:10.1190/1.1444921.
- Malagnini, L., A. Akinci, K. Mayeda, I. Munafo, R. B. Herrmann, and A. Mercuri (2012), Characterization of earthquake-induced ground motion from the L'Aquila seismic sequence of 2009, Italy, *Geophys. J. Int.*, *184*(1), 325–337, doi:10.1111/j.1365-246X.2010.04837.x.
- Matrullo, E., R. De Matteis, C. Satriano, O. Amoroso, and A. Zollo (2013), An improved 1-D seismic velocity model for seismological studies in the Campania–Lucania region (Southern Italy), *Geophys. J. Int.*, *195*, 460–473, doi:10.1093/gji/ggt224.
- Mavko, G., T. Mukerji, and J. Dvorkin (2009), Effective elastic media: Bounds and mixing laws, in *The Rock Physics Handbook, Second Edition: Tools for Seismic Analysis of Porous Media*, pp. 177–178, Cambridge Univ. Press, Cambridge, U. K.
- Michellini, A., and T. V. McEvilly (1991), Seismological studies at Parkfield, I, Simultaneous inversion for velocity structure and hypocenters using cubic B-splines parameterization, *Bull. Seismol. Soc. Am.*, *81*, 524–552.
- Mostardini, F., and S. Merlini (2004), Appennino centro-meridionale, Sezioni geologiche e proposta di modello strutturale, *Mem. Soc. Geol. Ital.*, *35*, 177–202.
- Morozov, I. B. (2008), Geometrical attenuation, frequency dependence of Q , and the absorption band problem, *Geophys. J. Int.*, *175*, 239–252, doi:10.1111/j.1365-246X.2008.03888.x.
- Nur, A., and J. R. Booker (1972), Aftershocks caused by pore fluid flow?, *Science*, *17*(4024), 885–887.
- Patanè, D., G. Barberi, O. Cocina, P. De Gori, C. Chiarabba, and C. (2006), Time-resolved seismic tomography detects magma intrusions at Mount Etna, *Science*, *313*, 821–823, doi:10.1126/science.1127724.
- Pride, S. R. (2005), Relationships between seismic and hydrological properties, in *Hydrogeophysics*, pp. 253–290, Springer, Netherlands.
- Rietbrock, A. (2001), P wave attenuation structure in the fault area of the 1995 Kobe earthquake, *J. Geophys. Res.*, *106*(B3), 4141–4154, doi:10.1029/2000JB900234.
- Rovida, A., M. Locati, R. Camassi, B. Lollì, and P. Gasperini (Eds.) (2016), *CPT115, the 2015 version of the Parametric Catalogue of Italian Earthquakes*, Istituto Nazionale di Geofisica e Vulcanologia, doi:10.6092/INGV.IT-CPT115.
- Schmoker, J. W., and R. B. Halley (1982), Carbonate porosity versus depth: a predictable relation for south Florida, *AAPG Bull.*, *66*(12), 2561–2570.
- Shapiro, S. A., R. Patzig, E. Rothert, and J. Rindschwentner (2003), Triggering of seismicity by pore-pressure perturbations: Permeability-related signatures of the phenomenon, *Pure Appl. Geophys.*, *160*, 1051–1061.
- Stabile, T. A., C. Satriano, A. Orefice, G. Festa, and A. Zollo (2012), Anatomy of a microearthquake sequence on an active normal fault, *Sci. Rep.*, *2*, 410, doi:10.1038/srep00410.
- Trippetta, F., C. Collettini, M. R. Barchi, A. Lupattelli, and F. Mirabella (2013), A multidisciplinary study of a natural example of a CO_2 geological reservoir in central Italy, *Int. J. Greenhouse Gas Control*, *12*, 72–83, doi:10.1016/j.ijggc.2012.11.010.
- Vidale, J. E., and P. M. Shearer (2006), A survey of 71 earthquakes bursts across Southern California: Exploring the role of pore fluid pressure fluctuations and aseismic slip as driver, *J. Geophys. Res.*, *111*, B05312, doi:10.1029/2005JB004034.
- Wyllie, M. R. J., A. R. Gregory, and L. W. Gardner (1956), Elastic wave velocities in heterogeneous and porous media, *Geophysics*, *21*(1), 41–70.
- Zollo, A., L. D'Auria, R. De Matteis, A. Herrero, J. Virieux, and P. Gasparini (2002), Bayesian estimation of 2-D P -velocity models from active seismic arrival time data: imaging of the shallow structure of Mt Vesuvius (Southern Italy), *Geophys. J. Int.*, *151*, 566–582, doi:10.1046/j.1365-246X.2002.01795.x.
- Zollo, A., A. Orefice, and V. Convertito (2014), Source parameter scaling and radiation efficiency of microearthquakes along the Irpinia fault zone in southern Apennines, Italy, *J. Geophys. Res. Solid Earth*, *119*, 3256–3275, doi:10.1002/2013JB010116.